Colloidal Quantum-Dot Photodetectors Exploiting Multiexciton Generation

Vlad Sukhovatkin, *et al.*

Science **324**, 1542 (2009);
DOI: 10.1126/science.1173812

References and Notes

1. C. Waelkens *et al.*, *Astron. Astrophys.* **330**, 215 (1998).
2. K. Uytterhoeven *et al.*, *J. Phys. Conf. Ser.* **118**, 012077 (2008).
3. W. A. Dziembowski, A. A. Pamiatnykh, *Mon. Not. R. Astron. Soc.* **262**, 204 (1993).
4. M. Cantiello *et al.*, *Astron. Astrophys.* **499**, 279 (2009).
5. The CoRoT space mission, launched on 27 December 2006, has been developed and is operated by CNES, with the contribution of Austria, Belgium, Brazil, the European Space Agency (ESA) (Research and Scientific Support Department and Science Programme), Germany, and Spain.
6. M. Auvergne *et al.*, *Astron. Astrophys.*, http://arXiv.org/abs/0901.2206.
7. E. Michel *et al.*, *Science* **322**, 558 (2008).
8. F. Baudin, A. Gabriel, D. Gibert, *Astron. Astrophys.* **285L**, 29 (1994).
9. T. Morel, C. Aerts, *CoAst* **150**, 201 (2007).
10. M. A. Dupret, *Astron. Astrophys.* **366**, 166 (2001).
11. K. Belkacem *et al.*, *Astron. Astrophys.* **478**, 163 (2008).

12. K.B. acknowledges financial support from Liège University through the Subside Fédéral pour la Recherche. Part of this research was funded by the Belgian Prodex-ESA. L.L. has been partly supported by CNES. A.T. is Chercheur Qualifié at the Fonds National de la Recherche Scientifique (FNRS) and A.M. is Chargé de recherches FNRS.

Supporting Online Material

www.sciencemag.org/cgi/content/full/324/5934/1540/DC1
SOM Text
Figs. S1 to S5
References

5 February 2009; accepted 13 May 2009
10.1126/science.1171913

Colloidal Quantum-Dot Photodetectors Exploiting Multiexciton Generation

Vlad Sukhovatkin, Sean Hinds, Lukasz Brzozowski, Edward H. Sargent*

Multiexciton generation (MEG) has been indirectly observed in colloidal quantum dots, both in solution and the solid state, but has not yet been shown to enhance photocurrent in an optoelectronic device. Here, we report a class of solution-processed photoconductive detectors, sensitive in the ultraviolet, visible, and the infrared, in which the internal gain is dramatically enhanced for photon energies E_{photon} greater than 2.7 times the quantum-confined bandgap $E_{bandgap}$. Three thin-film devices with different quantum-confined bandgaps (set by the size of their constituent lead sulfide nanoparticles) show enhancement determined by the bandgap-normalized photon energy, $E_{photon}/E_{bandgap}$, which is a clear signature of MEG. The findings point to a valuable role for MEG in enhancing the photocurrent in a solid-state optoelectronic device. We compare the conditions on carrier excitation, recombination, and transport for photoconductive versus photovoltaic devices to benefit from MEG.

Multiexciton generation (MEG) refers to the creation of two or more electron-hole pairs per absorbed photon in a semiconductor (*1*). Colloidal quantum-dot materials in which MEG has been reported experimentally include PbS and PbSe (*2*), PbTe (*3*), CdSe (*4*), and Si (*5*). In bulk semiconductors, carrier multiplication has been observed repeatedly over the past five decades, both in elemental semiconductors such as germanium (*6*) and silicon (*7*) and also in lead chalcogenides (*8*), including the infrared-bandgap bulk semiconductor PbS (*9*). In the past year, experiments that carefully account for processes such as photoionization of nanoparticles during spectroscopic studies have evidenced the production of more than one exciton per photon (*10*) in colloidal quantum dots, with yields ranging from 1.1 to 2.4 excitons per photon (*10*) when the photon energy exceeds the MEG threshold near ~$E_{photon}/E_{bandgap} > 2.7$ (*11*), where E_{photon} is the photon energy and $E_{bandgap}$ is the quantum-confined bandgap.

MEG has been reported, based on all-optical spectroscopic data, not only in solution but also in thin solid films; however, in spite of numerous attempts with materials systems and photon energies reported to manifest MEG, neither the external quantum efficiency (EQE) nor the internal quantum efficiency (IQE) of the photocurrent in a device has been shown to exceed 100% (*12*–*20*). In particular, one careful and systematic study (*21*) recently explored whether a key signature of MEG—an IQE of greater than unity—was observable in the photocurrent of a low-bandgap PbSe colloidal quantum-dot photovoltaic device. Once reflection and absorption were carefully taken into account, IQEs approaching, but not exceeding, 100% were reported.

Recent reports (*22*) suggest that in some of the earlier spectroscopic studies, the apparent quantum yield of MEG was enhanced by photoionization in the presence of multiple excitons. The sequence of steps is depicted in Fig. 1. The generation of two excitons within one quantum dot (Fig. 1B) produces efficient Auger recombination; one exciton recombines, and one carrier associated with the other exciton is excited high within its band (Fig. 1C). Photoionization, in this instance known as Auger-assisted ionization (AAI), may occur when this excited charge carrier becomes trapped at or near the quantum dot's surface, resulting in a nanoparticle that possesses a long-lived net charge (Fig. 1D). The energetic Auger electron has a higher probability of being captured to a trap than does an already-thermalized electron (*23*) because it can more easily surmount the energetic barrier (such as a thin oxide on the nanoparticle surface), restricting access to a surface trap state.

Subsequent photogeneration of even a single exciton then results in the presence of a trion (an exciton plus a charge) that recombines rapidly, masquerading as MEG in recombination dynamics–based studies. Thus, MEG's time-resolved spectroscopic signatures are enhanced by photoionization. It should be emphasized that, at the low intensities of interest in MEG investigations, photoionization alone cannot masquerade as MEG and serves only to amplify the apparent quantum yield if MEG is already present.

Unfortunately, MEG combined with photoionization provides no advantages over MEG alone in the harvest of photovoltaic energy. Indeed, because trions resulting from photoionization accelerate recombination, they render even more challenging the extraction of MEG photocurrent from a photovoltaic device. To observe the benefits of MEG in the current extracted from a photovoltaic device, charge separation must occur before

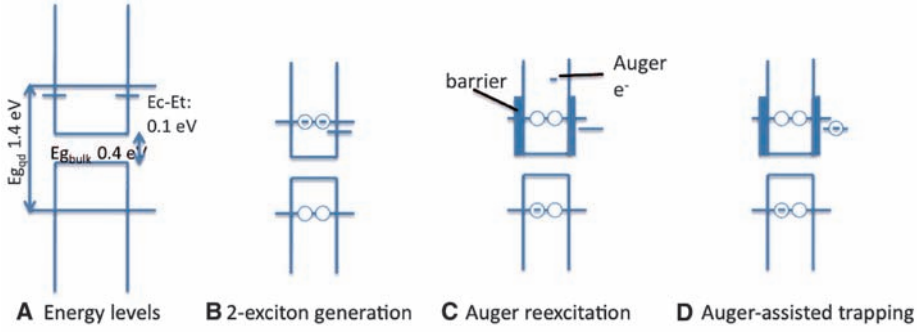

Fig. 1. MEG accompanied by photoionization. (**A**) Bands and trap levels for the quantum dots that were used. E_c is the quantum-confined conduction band edge, E_t is the trap energy, E_{gqd} is the quantum-confined bandgap, and E_{gbulk} is the constituent semiconductor's bulk bandgap. (**B**) Generation of a pair of excitons via photon absorption followed by carrier multiplication. (**C**) Auger-induced excitation of an electron to a higher-lying level concomitant with recombination of the other exciton. (**D**) Efficient trapping of the excited electron.

Department of Electrical and Computer Engineering, University of Toronto, Toronto, ON M5S 3G4, Canada.

*To whom correspondence should be addressed. E-mail: ted.sargent@utoronto.ca

Auger-accelerated multiexciton recombination. In PbS, for example, the biexciton lifetime is 50 ps and the triexciton lifetime is 30 ps (*24*). For a PbS photovoltaic device (*12*) with a typical built-in voltage of 0.35 V over a 100-nm-thick depletion region and for an electron and hole mobility of 1×10^{-3} cm^2/Vs measured in colloidal quantum-dot photovoltaic devices (*13*), the time for carriers to separate over ~5 nm (the interdot lengthscale) is on the order of 100 ps. Given the rapid rate of Auger recombination and the difficulty in dissociating excitons into distinct quantum dots, it is not surprising that the combination of materials parameters leading to greater-than-unity EQE or IQE in a photovoltaic device has yet to be conclusively observed.

We sought to identify a class of devices of applied interest in which telltale MEG signatures could be observed in the devices' photocurrents and in which photoionization would further improve, rather than detract from, performance. In photoconductive detectors (*25*), electron-hole pair generation is followed by the trapping of one type of carrier (such as electrons) and flow of the other (such as holes). If the flowing carrier can be recirculated (withdrawn from one contact and reinjected from the other) multiple times during the lifetime of the trapped carrier, then photoconductive gain results: Many charge carriers may be collected for every exciton generated.

In sum, photoconductors benefit from the capture of charge carriers to sensitizing centers, or traps, on the nanoparticle surface. We reasoned that they could therefore enjoy considerably enhanced electrical photocurrents when MEG and photoionization worked in concert. Thus, for $E_{photon} > \sim 2.7\ E_{bandgap}$, we expected that photoionization-enhanced MEG could considerably aid the trapping of charge carriers to sensitizing centers, leading to an improved signal-to-noise ratio that would be valuable in the sensitive detection of light. Because we worked with PbS nanoparticles that have quantum-confined bandgaps in the 750- to 1000-nm range, MEG enhancements were possible in the ultraviolet (UV).

Figure 1A depicts the bands of a typical set of PbS colloidal quantum dots that were used (*26*). PbS has a bulk bandgap of 0.4 eV; the effective bandgap rises to 1.4 eV through quantum confinement in the 2-nm-diameter dots investigated here. A shallow trap, resulting from $PbSO_3$ formed by surface oxidation of PbS (*27*), lies just below the first confined electron state. The use of devices (*28*) with a single trap-state lifetime facilitated the interpretation of the results presented.

The responsivity spectra are shown in Fig. 2B. By combining these data with careful measurements of the absorbance spectrum of the same film (Fig. 2A), we were able to determine the internal photoconductive gain of the device, which is plotted in Fig. 2C (*26*). Error analysis is presented in the figure caption.

Figure 2C reveals that the internal photoconductive gain is, as a function of wavelength, constant (spectrally flat) until 340 nm, a wavelength corresponding to a photon energy that is equal to 2.7 times the bandgap energy. At higher photon

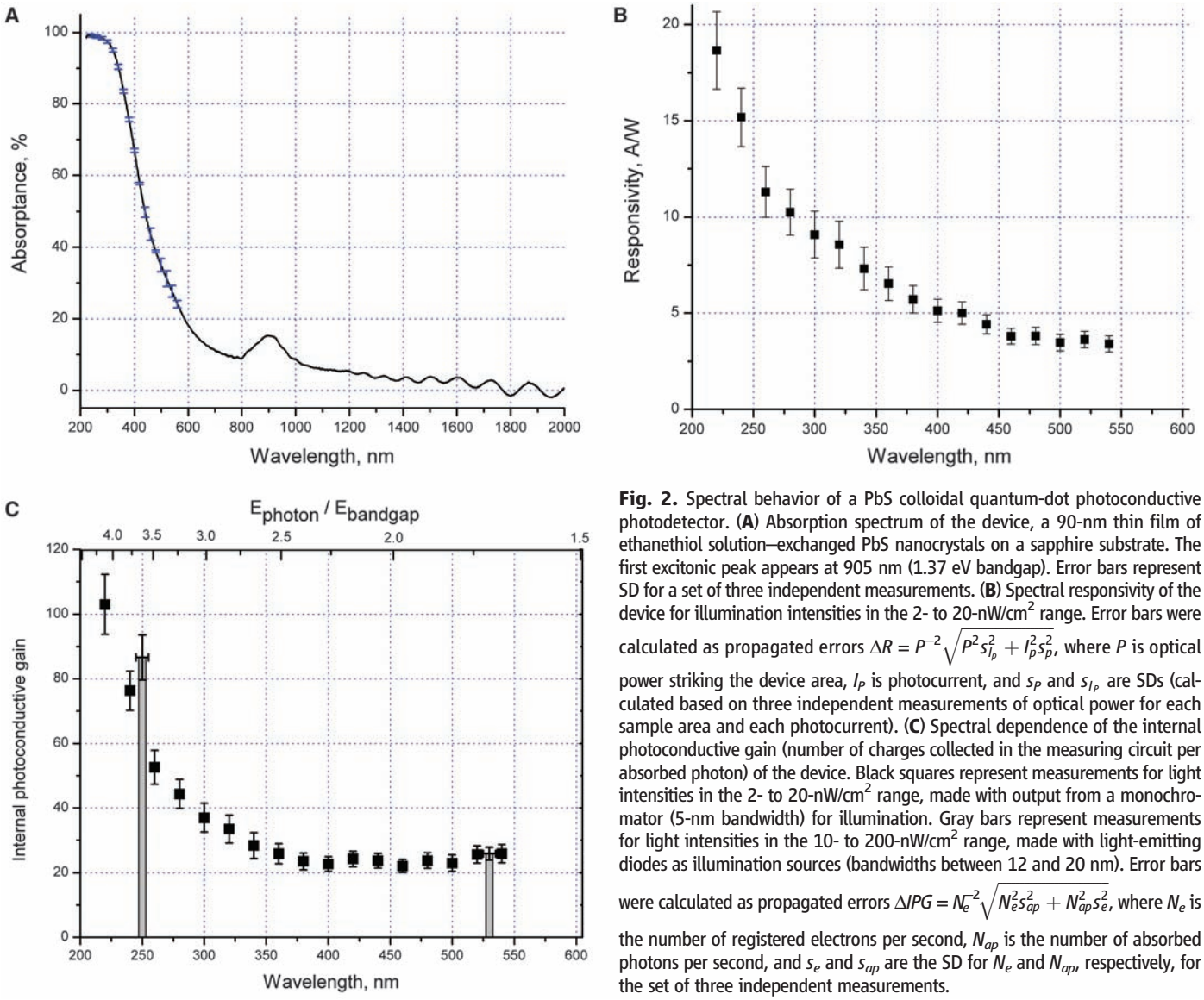

Fig. 2. Spectral behavior of a PbS colloidal quantum-dot photoconductive photodetector. (**A**) Absorption spectrum of the device, a 90-nm thin film of ethanethiol solution–exchanged PbS nanocrystals on a sapphire substrate. The first excitonic peak appears at 905 nm (1.37 eV bandgap). Error bars represent SD for a set of three independent measurements. (**B**) Spectral responsivity of the device for illumination intensities in the 2- to 20-nW/cm^2 range. Error bars were calculated as propagated errors $\Delta R = P^{-2}\sqrt{P^2 s_{I_p}^2 + I_p^2 s_P^2}$, where P is optical power striking the device area, I_P is photocurrent, and s_P and s_{I_p} are SDs (calculated based on three independent measurements of optical power for each sample area and each photocurrent). (**C**) Spectral dependence of the internal photoconductive gain (number of charges collected in the measuring circuit per absorbed photon) of the device. Black squares represent measurements for light intensities in the 2- to 20-nW/cm^2 range, made with output from a monochromator (5-nm bandwidth) for illumination. Gray bars represent measurements for light intensities in the 10- to 200-nW/cm^2 range, made with light-emitting diodes as illumination sources (bandwidths between 12 and 20 nm). Error bars were calculated as propagated errors $\Delta IPG = N_e^{-2}\sqrt{N_e^2 s_{ap}^2 + N_{ap}^2 s_e^2}$, where N_e is the number of registered electrons per second, N_{ap} is the number of absorbed photons per second, and s_e and s_{ap} are the SD for N_e and N_{ap}, respectively, for the set of three independent measurements.

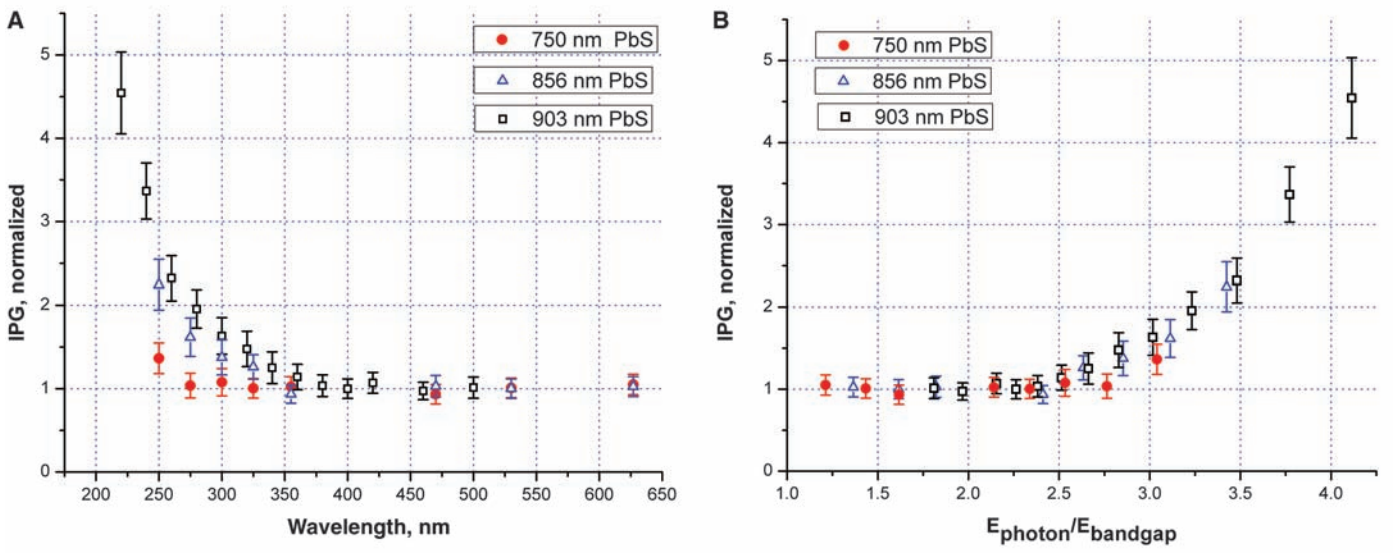

Fig. 3. Internal photoconductive gain spectra of three devices having different quantum-confined bandgaps. The left spectra (**A**) are plotted in absolute wavelength, whereas the right spectra (**B**) are plotted in (unitless) $E_{photon}/E_{bandgap}$. It is evident that $E_{photon}/E_{bandgap}$, and not absolute E_{photon}, is the quantity that drives the internal photoconductive gain spectral behavior. This finding is incompatible with direct ionization and compatible with MEG. Error bars were calculated as in Fig. 2.

energies, the internal gain rises sharply into the UV spectral range. The internal gain reaches a value of 100 ± 10 at 220-nm wavelength (~4.1 times the bandgap energy) as compared with its value of 25 ± 3 in the spectrally flat region below 2.7 times the bandgap energy.

Motivated by the fact that these results were consistent with, and even suggestive of, a role for MEG, we sought an experiment that could reveal MEG's unambiguous spectral signature: a universal quantum-yield curve dependent only on $E_{photon}/E_{bandgap}$. We built three devices using differently sized colloidal quantum dots having correspondingly different bandgaps (*26*). The devices' internal gain spectra, obtained exactly as in Fig. 2, are reported in Fig. 3.

We now discuss additional sets of controls that address potential artifactual explanations of these findings. One hypothesis is that trap states could be nonuniformly distributed throughout the film and perhaps clustered closer to the air-film interface; shorter-wavelength light would then be substantially absorbed in these denser and deeper trap regions. However, we compared internal-gain spectra for devices illuminated from the top versus the bottom and found no dependence in the curves of Figs. 2 and 3 on the side of optical incidence (fig. S3). A second hypothesis is that, in the case of short-wavelength illumination, excited carriers could be captured directly to traps during the subpicosecond time frame before relaxation to the quantum-confined band edge without need of MEG and AAI. This direct-ionization picture is incompatible with the observed universal normalized $E_{photon}/E_{bandgap}$ spectral dependence in Fig. 3; instead, it predicts that trapping efficiency should depend on E_{photon}, the barrier to electron escape, and the set of trap states available. To vary the trap states, we aged a series of devices in air to alter their trap-state densities and depths. We confirmed that the trap distribution had changed, observing an increase in dark current and the emergence of additional longer–time scale temporal components in the photoresponse that was consistent with the introduction of new and deeper traps. Despite these major changes in trap-state populations, we found that the spectral gain–dependence of Figs. 2 and 3 was preserved. Taken together, these observations suggest that carrier multiplication occurs more rapidly than either intersubband relaxation or the capture of excited carriers to traps.

We conclude with a brief discussion of the relevance to short-wavelength imaging of the devices we report here. A light sensor suited for imaging must simultaneously provide high responsivity combined with rapid temporal response (<1/15 s). Reports of UV-sensing elements based on solution-processed materials have, however, provided either promising sensitivity (61 A/W) but hundreds-of-seconds temporal response (*29*) or else fast response but few-milliamperes-per-Watt UV responsivity (*30*). The devices we report here are UV photodetectors with high responsivities of 18 A/W that at the same time offer an imaging-compatible 20-ms response time. The devices provide a 1000-fold improvement in gain-bandwidth product in solution-processed UV photodetection relative to previous reports. Compared with digital-imaging chips based on silicon photodiodes limited to at most one photoelectron per photon (thereby necessitating use of an extremely low-noise readout scheme), the devices we report here offer large gains that facilitate high-sensitivity low-light imaging.

References and Notes

1. A. J. Nozik, *Chem. Phys. Lett.* **457**, 3 (2008).
2. R. J. Ellingson *et al.*, *Nano Lett.* **5**, 865 (2005).
3. J. E. Murphy *et al.*, *J. Am. Chem. Soc.* **128**, 3241 (2006).
4. R. D. Schaller, M. Sykora, S. Jeong, V. I. Klimov, *J. Phys. Chem. B* **110**, 25332 (2006).
5. M. C. Beard *et al.*, *Nano Lett.* **7**, 2506 (2007).
6. J. Tauc, *J. Phys. Chem. Solids* **8**, 219 (1959).
7. S. Kolodinski, J. H. Werner, T. Wittchen, H. J. Queisser, *Appl. Phys. Lett.* **63**, 2405 (1993).
8. N. S. Baryshev, M. P. Shchetinin, S. P. Chashchin, Y. S. Kharionovskii, I. S. Aver'yanov, *Sov. Phys. Semicond.* **8**, 192 (1974).
9. A. Smith, D. Dutton, *J. Opt. Soc. Am.* **48**, 1007 (1958).
10. M. C. Beard *et al.*, *Nano Lett.* **9**, 836 (2009).
11. A. J. Nozik, *Chem. Phys. Lett.* **457**, 3 (2008).
12. K. W. Johnston *et al.*, *Appl. Phys. Lett.* **92**, 122111 (2008).
13. K. W. Johnston *et al.*, *Appl. Phys. Lett.* **92**, 151115 (2008).
14. G. I. Koleilat *et al.*, *ACS Nano* **2**, 833 (2008).
15. E. J. D. Klem, D. D. MacNeil, P. W. Cyr, L. Levina, E. H. Sargent, *Appl. Phys. Lett.* **90**, 183113 (2007).
16. M. Law *et al.*, *J. Am. Chem. Soc.* **130**, 5974 (2008).
17. J. M. Luther *et al.*, *ACS Nano* **2**, 271 (2008).
18. A. Luque, A. Martí, A. J. Nozik. *MRS Bull.* **32**, 236 (2007).
19. X. Jiang *et al.*, *J. Mater. Res.* **22**, 2204 (2007).
20. E. H. Sargent, *Nat. Photon.* **3**, 325 (2009).
21. M. Law *et al.*, *Nano Lett.* **8**, 3904 (2008).
22. J. A. Mcguire, J. Joo, J. M. Pietryga, R. D. Schaller, V. I. Klimov, *Acc. Chem. Res.* **41**, 1810 (2008).
23. V. Klimov *et al.*, *Conference on Quantum Electronics and Laser Science (QELS), Technical Digest Series* (IEEE, San Francisco, 2000).
24. E. Istrate *et al.*, *J. Phys. Chem. B* **112**, 2757 (2008).
25. G. Konstantatos *et al.*, *Nature* **442**, 180 (2006).
26. Materials and methods are available as supporting material on *Science* Online.
27. G. Konstantatos, L. Levina, A. Fischer, E. H. Sargent, *Nano Lett.* **8**, 1446 (2008).
28. S. Hinds *et al.*, *Adv. Mater.* **20**, 4398 (2008).
29. Y. Jin, J. Wang, B. Sun, J. C. Blakesley, N. C. Greenham, *Nano Lett.* **8**, 1649 (2008).
30. E. Mutlugun, I. M. Soganci, H. V. Demir, *Opt. Express* **16**, 3537 (2008).

31. This publication was based on work supported in part by an award from the King Abdullah University of Science and Technology, by the Natural Sciences and Engineering Research Council of Canada, by the Canada Research Chairs, and by the Canada Foundation for Innovation and the Ontario Innovation Trust.

Supporting Online Material

www.sciencemag.org/cgi/content/full/324/5934/1542/DC1
Materials and Methods
Figs. S1 to S3
References

19 March 2009; accepted 19 May 2009
10.1126/science.1173812